MANCHESTER 1824

The University of Manchester

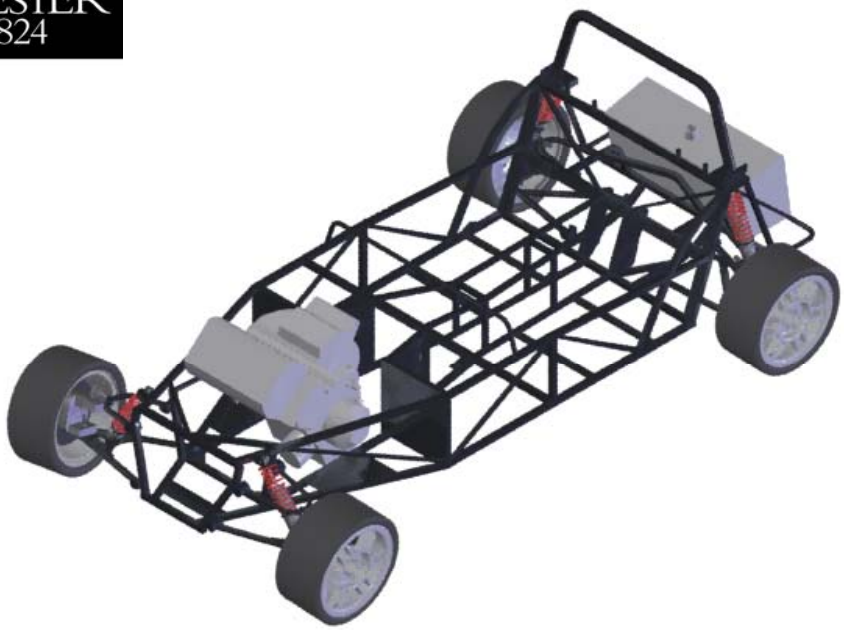

DESIGN IMPROVEMENT STUDY OF A KIT CAR SUSPENSION AND CHASSIS ARRANGEMENT

3RD Year MEng Project by Lee Comerford

Supervisor: Dr. J. Harrigan

Synopsis:15/07/05

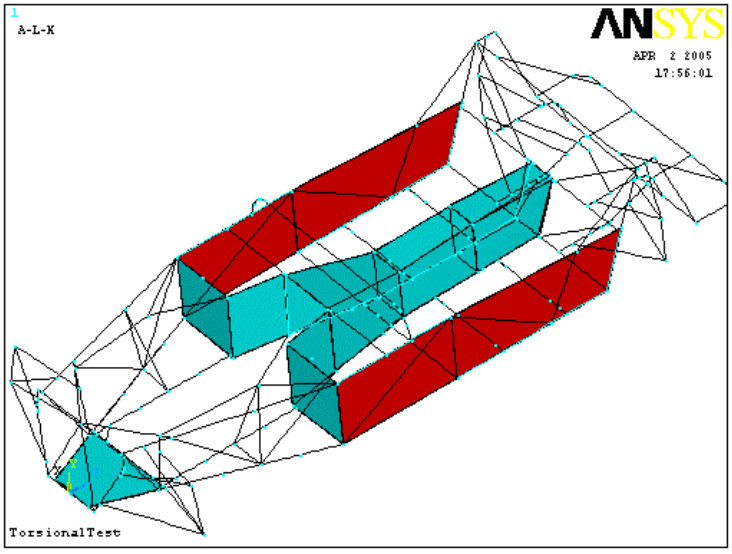

1. INTRODUCTION

AGM Sportscars is a newly formed manufacturer of exotic sports cars. The company's latest model; the WLR (Figure 4) is sold as a kit car and is notorious for the installation of powerful engines. This has raised customer concerns over the strength and stiffness of the suspension and chassis arrangement. The WLR chassis is based on a Lotus 7 inspired space-frame (Figure 1), the design of which had remained unchanged in thirty years despite engine power increases of over 300%. The project had the following objectives:

1. Derive formulae to quantify the loads imposed on the suspension and chassis arrangement;
2. Validate the results;
3. Estimate the working deflections of both the suspension components and chassis space-frame in operation;
4. Suggest a new and improved suspension and chassis design by limiting these deflections and any other means judged necessary.

Details of the work carried out to achieve these objectives are summarized in this synopsis. The report documents the definition of the loading experienced by the suspension and chassis (Load Cases), structural analysis (Finite Element Analysis), validation of the analysis and details of modifications carried out. The effect of these modifications is then assessed through real-life loading scenarios (Working Deflections).

2. LOAD CASES

All forces experienced by a car originate at the small contact patches between the tyre and the road surface and follow a path through the suspension components and into the chassis (Figure 2). The forces acting on the WLR at the limit of the tyres traction were considered in the analysis.

A static load was applied to the chassis representative of the true dynamic loading by multiplying by a dynamic factor z where z indicates the extremity of the maneuver in units g of acceleration (a).

$$F_{Dynamic} = F_{Static} \times a / g = F_{Static} \times z$$

So, the static loads in the three planes are (Figure 4).

$$F_x = z_x M_u g \qquad F_y = z_y M_u g \qquad F_z = z_z M_u g$$

Where M_u is the total unsprung mass.

The dynamic factors were obtained by fitting accelerometers in the x, y and z planes and a data logger to the WLR and subjecting the car to extreme driving conditions. Maximum lateral acceleration was obtained in a skid-pan test; maximum longitudinal acceleration was obtained from rest and in emergency braking; maximum vertical acceleration was obtained by tackling rough terrain. Figure 3 illustrates typical data for the traverse around an oval track. A summary of the g-forces experienced is provided in Table 1.

For the purpose of the Finite Element Model, boundary conditions were required at the car wheels. Static wheel loads were calculated by application of Newton's Second Law (NSL) and these were then multiplied by z to represent the dynamic situation. The load cases considered were vertical bending from the vehicles internal components, pure torsion, combined bending and torsion, lateral loading, longitudinal loading, asymmetric loading and finally engine torque reaction.

It was also necessary to measure the loads experienced by the wishbones and this was achieved by fitting strain gauges (Figure 5) whereby circuit A measured transverse direct compression and tension and circuit B measured pure bending. By calibrating the wishbone (Figure 7) a direct relationship with wheel longitudinal and lateral loading was established. The 'Analogue 5' graph in Figure 6 represents the amplified voltage produced by circuit B during the oval track traverse. The largest strain occurred at 67.5 seconds when the driver lost control of the car and veered onto rough terrain, causing sudden deceleration. The voltage recorded here was 1.16V, which corresponds to a braking load of 592.6N.

Additionally, the wishbone loads were obtained from an extension of the NSL analysis. For example, when the car brakes the longitudinal force at the tyre contact patch creates a ‘brake force lever’ which attempts to turn the wheel. This is reacted by the upper and lower wishbones of the suspension system as in Figure 8. The longitudinal and lateral loads calculated in this manner are summarized in Tables 2 and 3 respectively. It was found that the NSL predictions were greater in magnitude than those read by the strain gauge circuits.

3. THE FINITE ELEMENT MODEL

Manual structural analysis of the suspension and chassis proved time consuming and inaccurate. Rather, a Finite Element approach was adopted which provided a repeatable method for analyzing changes in the topological layout.

There were two primary areas of concern. The upper front wishbone required a detailed plastic analysis in ABAQUS and was imported directly from Solid Works as an IGES file type. The solid was meshed with tetrahedral elements (Figure 9) and the chassis was assumed infinitely stiff in order that the suspension pivot points on the wishbone could be fixed to provide adequate boundary conditions. Applying maximum braking forces to the wishbone resulted in significant plastic deformation, Figure 10 illustrates stresses of over 200Mpa (the yield stress for mild steel) at the bends of the wishbone. Additionally, the maximum braking load caused large longitudinal deflection of the knuckle which is highly undesirable because it changes the geometry of the suspension, making the car difficult to handle.

After attempts to import the full chassis model into ABAQUS it soon became evident that another approach was necessary. ANSYS provides a feature whereby a three dimensional frame can be drawn by lines through the centre points of the members and then a cross-section assigned afterwards. In this way, simplex rather than complex elements are used, dramatically cutting processing time. The elements employed to create the full chassis model are provided in Table 4.

4. VALIDATION

The wishbone model was validated by comparison of the knuckle deflection from a known braking load, both in ABAQUS and experimentally (Figure 7). It was found that the model did underestimate the deflection of the actual wishbone significantly however ABAQUS still proved a useful tool to achieve relative improvement.

A prototype chassis was tested for its value of global torsional stiffness (Figure 11) which was found to be 676Nm/degree. This is of order lower than the average commercial vehicle. In order to validate the ANSYS model, the testing procedure was simulated within ANSYS (Figure 12) and it was found that ANSYS over predicted the stiffness of the chassis by 13%.

5. MODIFICATIONS

Only a change in the topological layout would provide adequate reduction in stress and deflections in the wishbone. Since the modification could not adjust the kinematics of the suspension geometry, the solution was to simply triangulate the wishbone and remove the slant from the front bulkhead in order to generate clearance around the shock absorber (Figure 13). This lowered the maximum stress to a level below the yield stress of the mild steel and limited longitudinal knuckle deflection to 0.7mm.

Modification of the chassis required a more detailed approach:

1. Improve the stiffness by adjusting the topological layout;
2. Calculate actual working load deflections for original and modified chassis;
3. Optimize the weight of the chassis by material and geometry considerations.

In normal use the chassis will operate well below the yield stress of the mild steel. Stiffness is the critical feature that must be retained in order for the car to handle well. In particular, the torsional stiffness of the chassis down the longitudinal axis is of most importance so a repeatable loading condition was created to test this. The model was constrained at the rear wheels and an arbitrary moment applied at the front wheels as

shown in Figure 14. A second loading condition was created to represent engine torque and involved constraining the chassis at the engine mounting positions and twisting the chassis at the differential mounting points as shown in Figure 15. In both load cases the chassis deflection was measured at the suspension pick-up point since this is where it is desirable to have deflections minimal.

It is useful to represent the chassis as a number of spring elements between the front and rear bulkheads. Each section has its own stiffness and contributes to the global stiffness of the chassis.

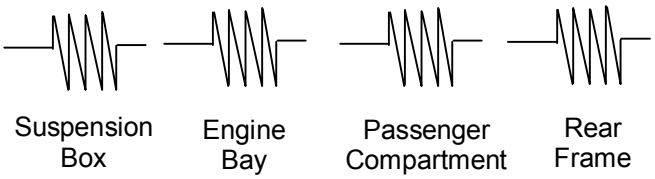

By viewing the deformed chassis in ANSYS it was clear that the troublesome areas were the suspension box, engine bay and passenger compartment which were effectively open containers and very susceptible to large deflections. Modifications were suggested beginning at the front of the chassis and are illustrated in Figures 16 to 26. The increase in stiffness to the torsional and engine torque load cases is shown in Tables 5 and 6. The technique employed was to close the open sections by triangulation or stressed skin. All added beams were mild steel 25mm, 16 gauge (1.6mm thickness) RHS and added cladding was 16 gauge mild steel plate.

The fully modified chassis is illustrated in Figure 27. Added members are highlighted in red and added cladding in yellow, removed members in green. The features combine to add 661% torsional stiffness to the chassis. This is an increase from 576Nm/degree to 4785Nm/degree. Given that ANSYS over-predicts the stiffness by 13% the modified chassis has a true stiffness of 4163 Nm/degree. Due to the effective rigid link on the floor of the engine bay from the engine installation, the vehicle stiffness is actually increased by a further 223%, giving rise to a vehicle stiffness of 5336Nm/degree.

6. WORKING DEFLECTIONS

The next stage in the structural analysis was to estimate the working deflections of the chassis under real loading conditions to meet certain requirements:

i) Mid-span working deflections should not exceed 2mm;
ii) Structural deflection at the suspension pick-up points should be limited to less than 1mm;
iii) Stress due to static load x Dynamic factor <=2/3 x yield stress.

Numerous problems were encountered when attempting to simulate the actual chassis loading conditions. If the loads were applied to the wheels, the chassis needed to be constrained which was unrealistic and also over-estimated the global stiffness. The most accurate way (within the capabilities of ANSYS) was to constrain the wheels and apply the internal loads to the chassis. This was made possible by Newton's Third Law. The force applied to the driver and engine by the wheel loads transferring through the chassis for example is equal and opposite to the force applied by the driver and engine to the chassis.

The most severe chassis deflections occurred from bending, combined bending and torsion and engine torque. The vertical bending load case is shown in Figure 28 and the deflection plots for the normal and modified chassis are provided in Figures 29 and 30. There is significantly less deflection in the modified chassis, particularly around the engine bay region. Tables 7 and 8 contain all the working deflections and it is clear that a large improvement results. In all but one case the deflections are brought within adequate magnitude of the specification.

7. CONCLUSION

All objectives were met successfully. Working loads were calculated by theory and validated by experimentation; by accelerometers for the chassis loads and strain gauge measurements for the wishbone loads.

The strength and stiffness of the suspension arrangement was increased significantly by a very simple modification and the stiffness of the chassis was improved by over 600%. The chassis modifications present a very small weight sacrifice due to the removal of ten redundant members around the transmission tunnel (Figure 25) and add minimal complication to manufacture.

The chassis with modifications went on sale on the 1st May 2005 at Stonely kit car show.

8. TABLES

Test	G-Force (g)		
	Longitudinal	Lateral	Vertical
Oval track traverse	0.9	1.1	-
Acceleration and emergency brake test	1.15	-	-
Skid pad test 1	0.22	1.2	-
Skid pad test 2	0.25	1.2	-
Skid pad test 3	0.55	1.2	-
High speed run	-	-	0.9

Table 1: G-force data for extreme driving conditions

Load Case	Longitudinal Loads (N)					
	F_F	F_{FU}	F_{FL}	F_R	F_{RU}	F_{RL}
Braking	5174.6	3022.2	5609.5	4253.2	2484.0	4610.6
Accelerating	-	-	-	510.5	-	-

Table 2: Maximum longitudinal traction and wishbone loads predicted by NSL

Load Case	Lateral Loads (N)					
	Y_F	Y_{FU}	Y_{FL}	Y_R	Y_{RU}	Y_{RL}
Right Corner	4174.8	2438.3	4525.7	3253.3	1900.1	3526.8
Left Corner	4174.8	-2438.3	-4525.7	3253.3	-1900.1	-3526.8

Table 3: Maximum lateral traction and wishbone loads predicted by NSL

Element Name	Use
Beam4	Rectangular Hollow Section (RHS) for the majority of chassis members. Solid rectangular beam for seat and petrol tank bracing.
Pipe16	Tubing for the steering column and diagonal members.
Link8	Tension/compression links for the suspension
Shell63	All cladding used in the model.

Table 4: Elements used in the full chassis model in ANSYS

Description	Deflection (mm)	Stiffness (Nm per degree)	Cumulative Increase (%)
Standard chassis	10.80	576.11	
Front bulkhead triangulation 1	10.10	615.70	6.87
Front bulkhead triangulation 2	9.92	626.73	8.79
Wishbone mount triangulation 1	9.45	658.08	14.23
Wishbone mount triangulation 2	9.29	669.42	16.20
Suspension box plated floor	8.29	749.81	30.15
Optional cross brace	5.63	1104.25	91.67
Engine bay member R	3.46	1795.67	211.69
Short diagonals across engine bay	5.38	1156.42	100.73
Longitudinal strengtheners, engine bay	6.23	998.83	73.38
Y-braces	4.76	1305.46	126.60
Y-braces plus cross-member	4.70	1322.28	129.52
Engine bay side triangulation	4.67	1332.17	131.24
Engine bay mount triangulation	4.68	1327.93	130.50
Plate transmission tunnel	1.70	3649.28	533.44
Plate transmission tunnel, remove redundant members	1.75	3543.62	515.10
Side panels	1.56	3976.50	590.24
Additional floor traverse members	1.56	3984.91	591.70
Widening the chassis	1.42	4384.52	661.06
Adding the engine	1.10	5668.00	-

Table 5: Increase in torsional stiffness as a result of the chassis modifications

Description	Deflection (mm)	Stiffness (Nm per degree)	Cumulative Increase (%)
Standard chassis (with suspension box modifications)	2.23	649.19	-
Y-braces	1.89	765.68	17.94
Engine bay side triangulation	1.52	952.13	46.66
Engine mount triangulation 1	1.51	958.60	47.66
Engine mount triangulation 2	1.36	1061.02	63.44
Engine mount triangulations 1 and 2	1.34	1076.34	65.80
Plate transmission tunnel	0.50	2896.00	346.09
Plate transmission tunnel and remove redundant members	0.53	2700.25	315.94

Table 6: Increase in stiffness in reaction to engine torque as a result of the chassis modifications

Load Case	Deflection (mm)	
	Mid-span	Shock pick-up
Bending (y)	3.09	0.50
Torsion plus bending (y)	17.72	31.95
Lateral (x,y)	1.18,0.26	1.04,1.39
Engine torque reaction (y)	2.09	2.23
Engine torque reaction plus bending (y)	3.89	0.61

Table 7: Working deflections of the original chassis

Load Case	Deflection (mm)	
	Mid-span	Shock pick-up
Bending (y)	1.81	0.37
Torsion plus bending (y)	4.50	6.61
Lateral (x,y)	0.36,0.102	0.33,0.44
Engine torque reaction (y)	2.20	1.49
Engine torque reaction plus bending (y)	2.62	0.52

Table 8: Working deflections of the modified chassis

9. FIGURES

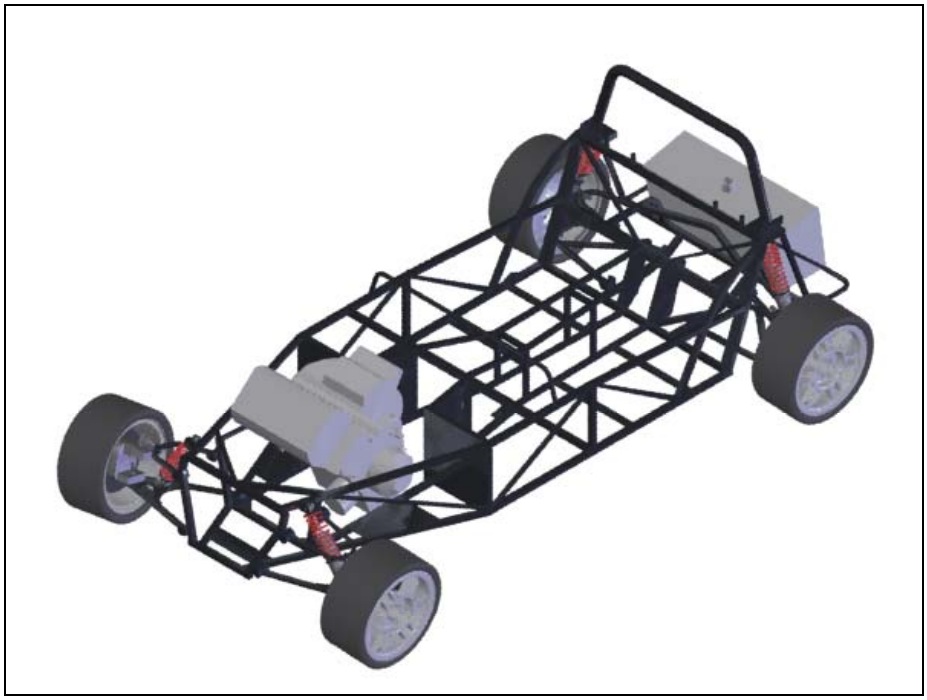

Figure 1: Model of the WLR chassis and some accompanying components in Solid Works

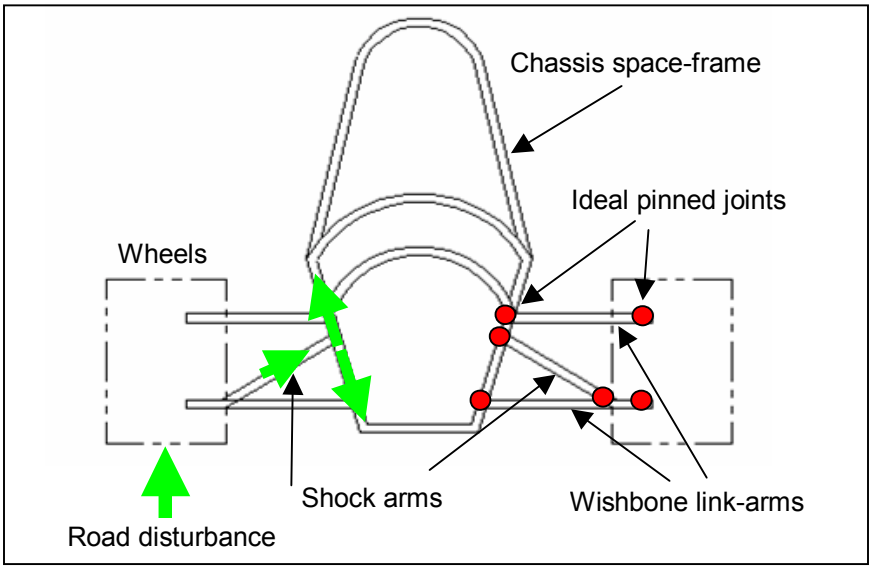

Figure 2: Transfer of load from the wheel to the chassis

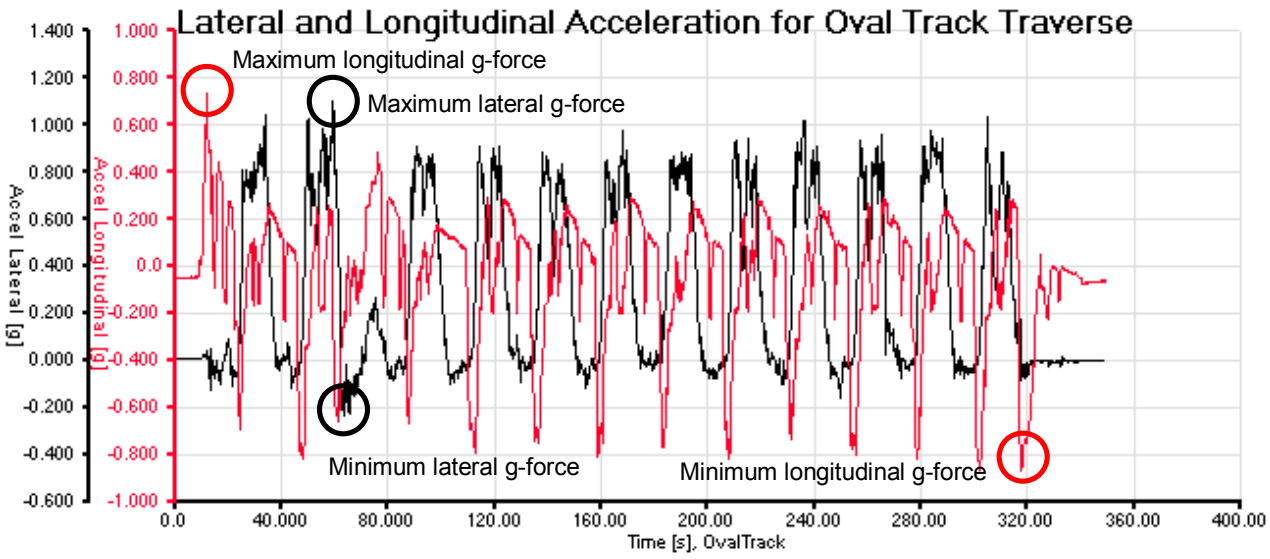

Figure 3: Lateral and Longitudinal acceleration for the oval track traverse

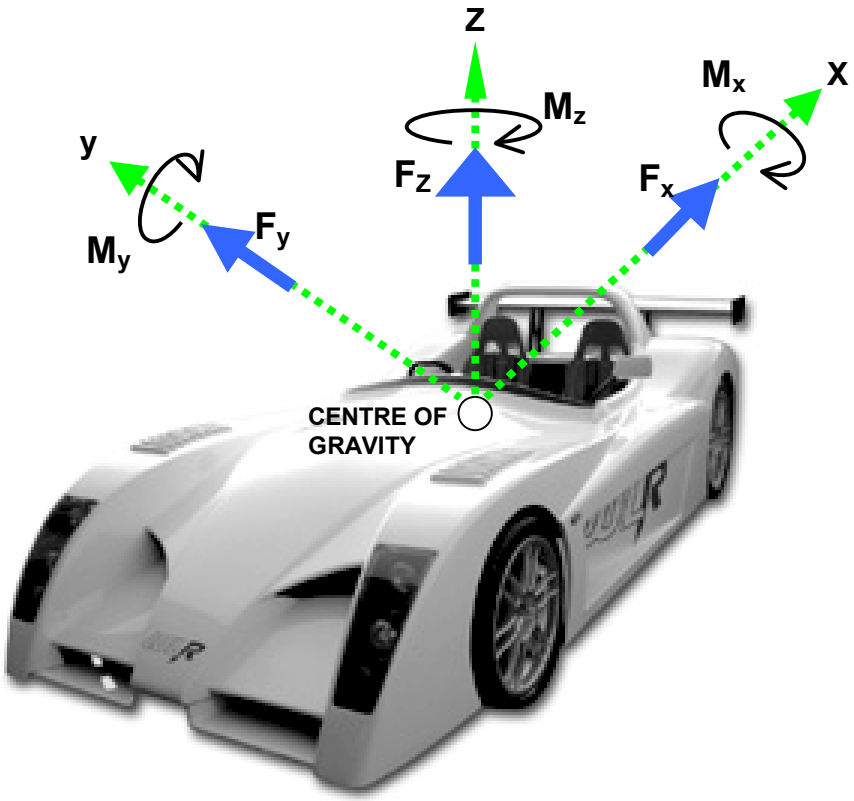

Figure 4: Car axis system

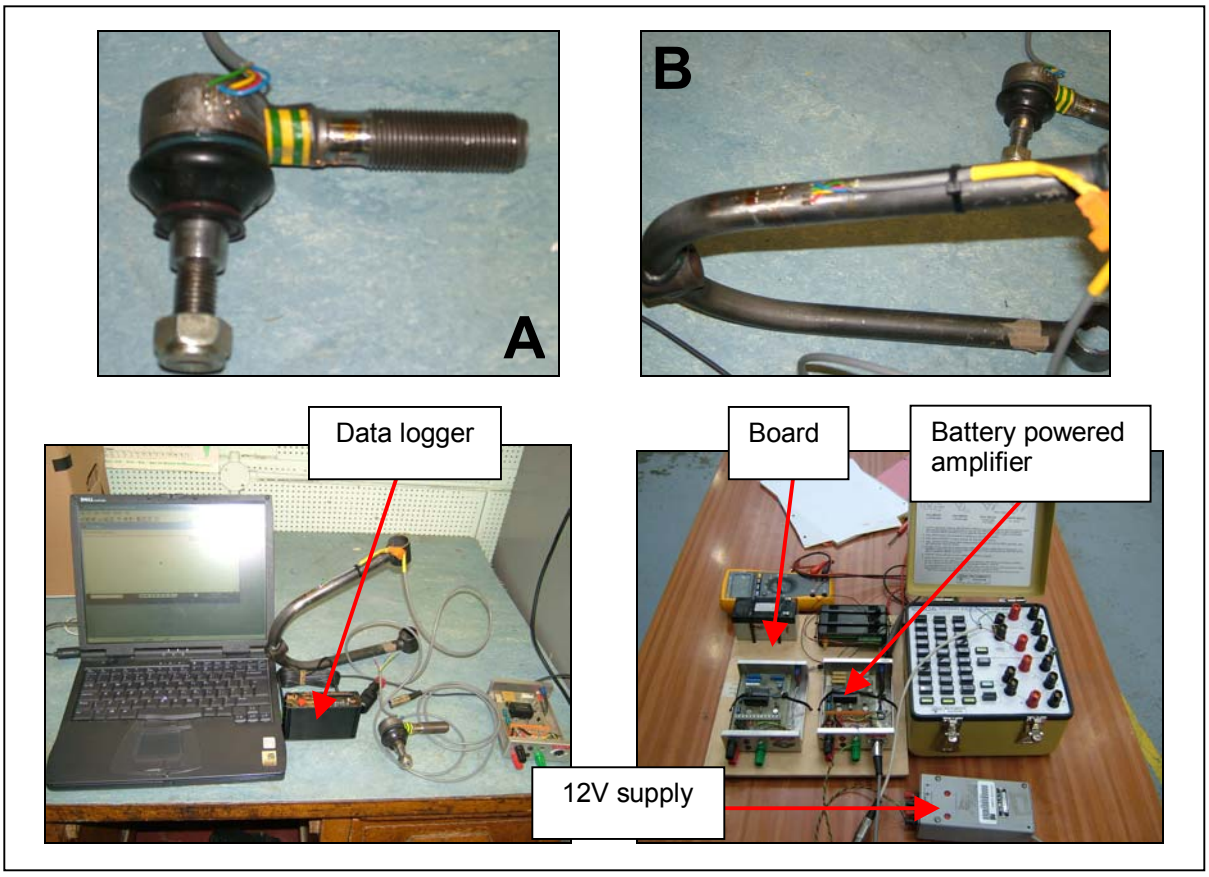

Figure 5: Strain gauges on the upper knuckle (A) and wishbone arm (B)

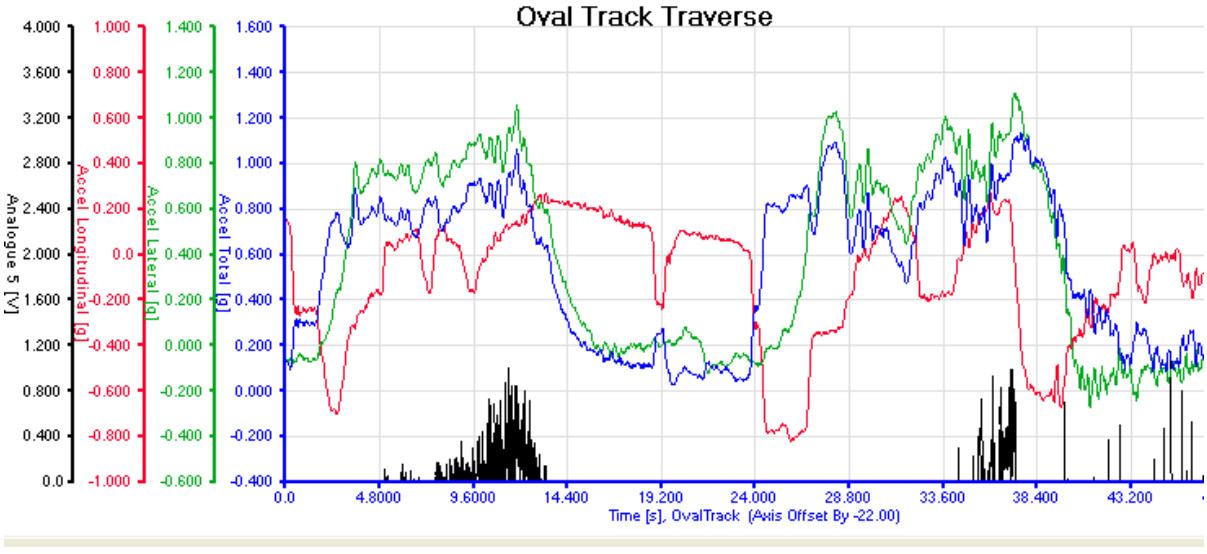

Figure 6: Wishbone circuit (B) output (Analogue 5) from the oval track traverse

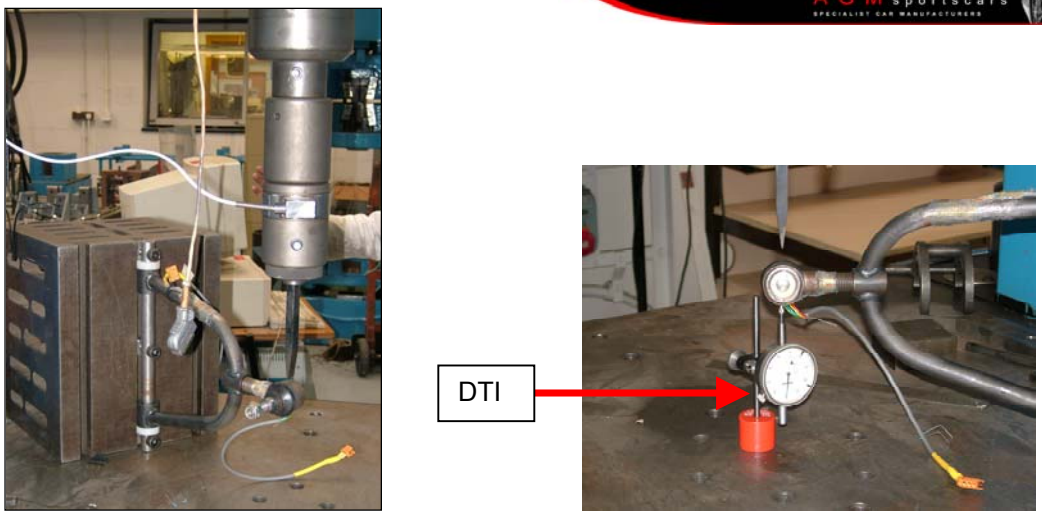

Figure 7: Calibrating circuit B

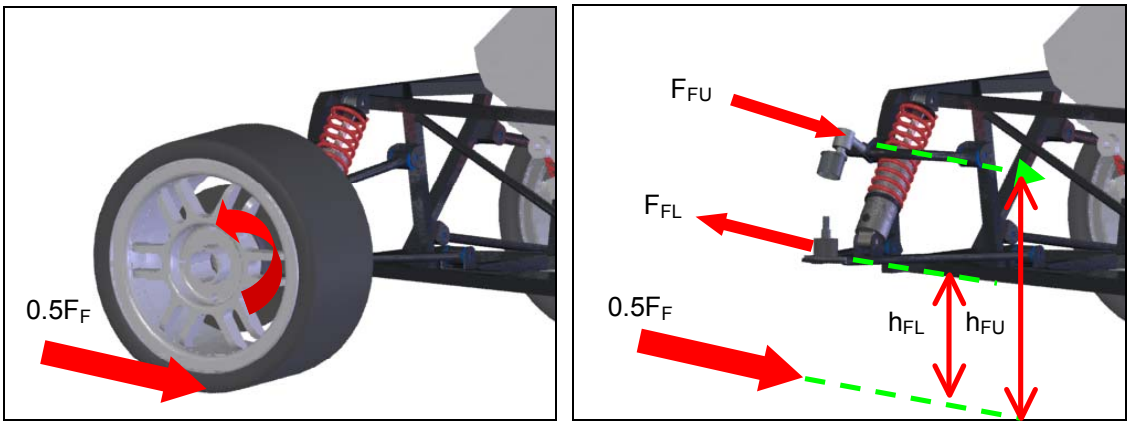

Figure 8: The force lever created by braking

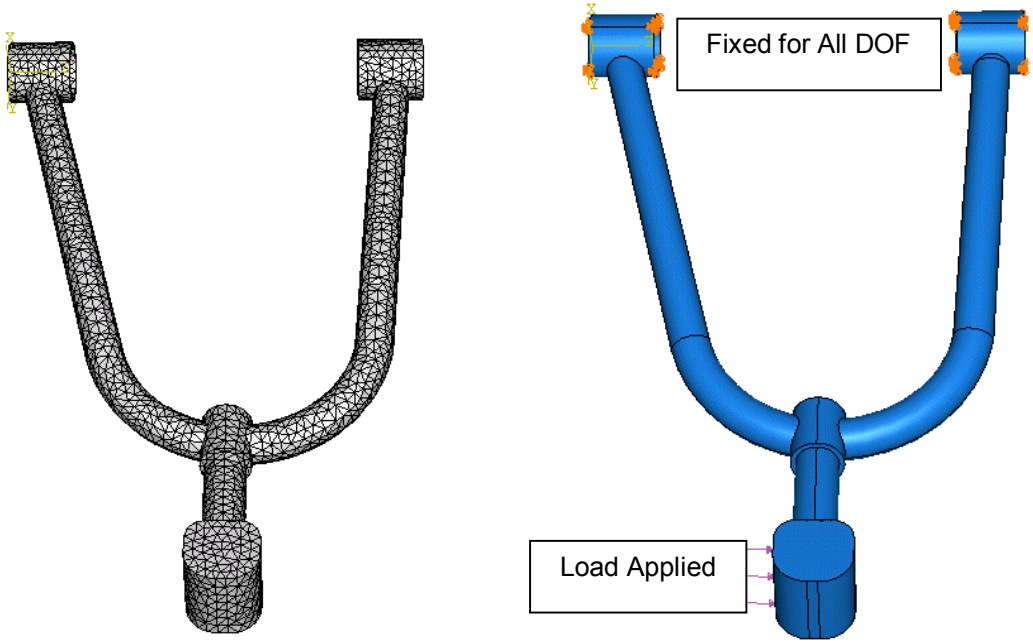

Figure 9: Meshing and applying boundary conditions to the wishbone model

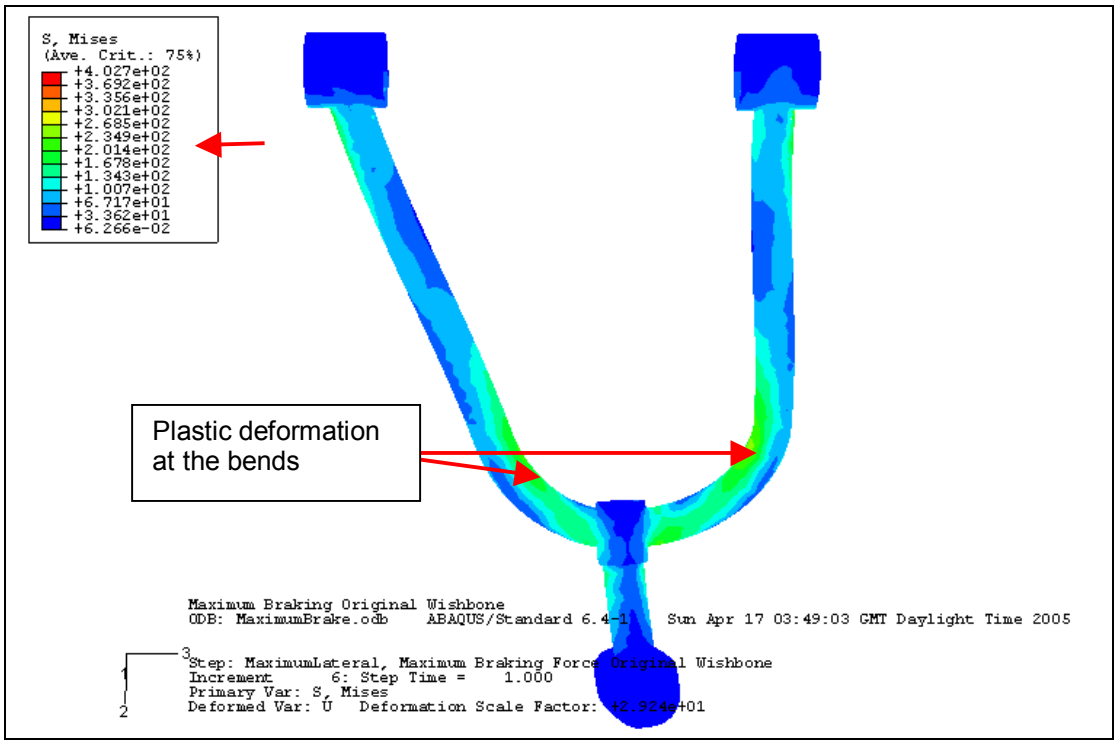

Figure 10: Von Mises stress plot for the original wishbone subjected to maximum braking

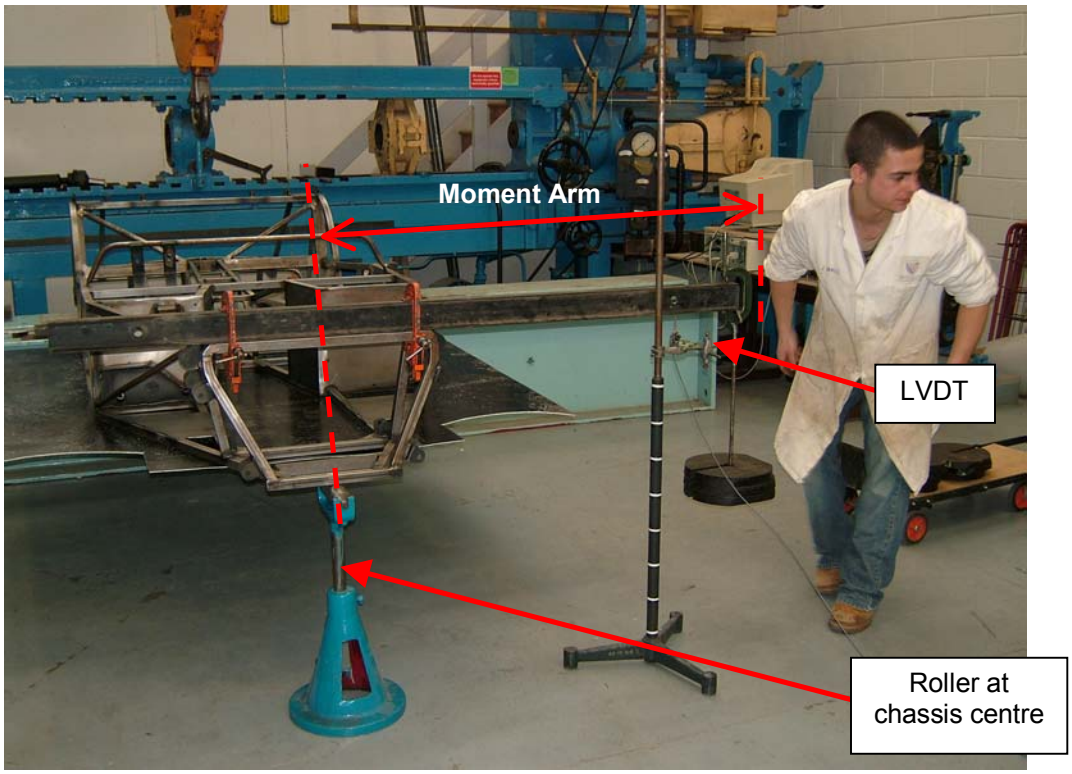

Figure 11: Testing a prototype chassis for its value of global torsional stiffness

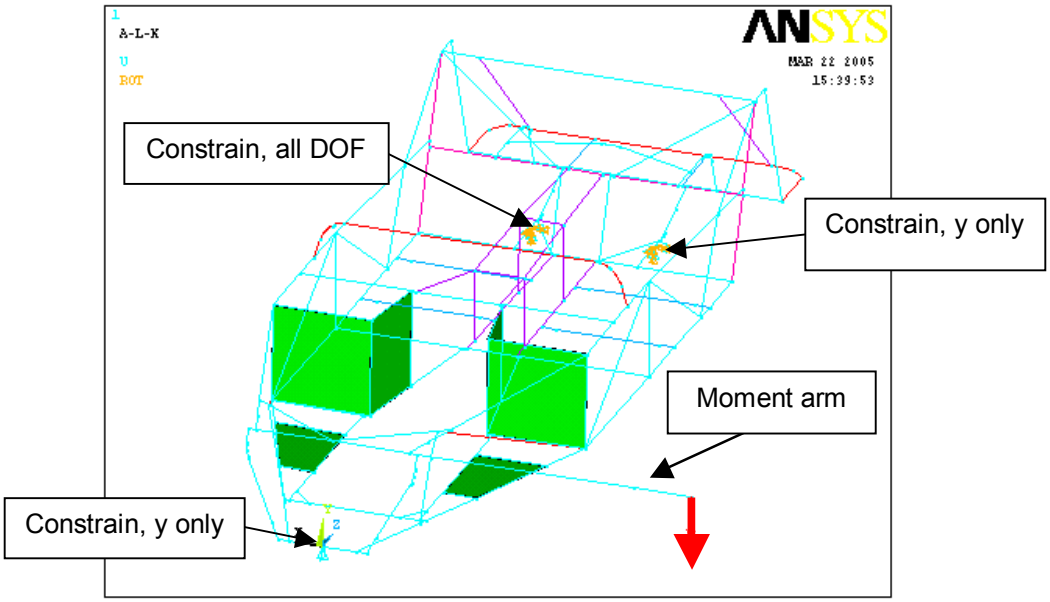

Figure 12: Validating the chassis full model

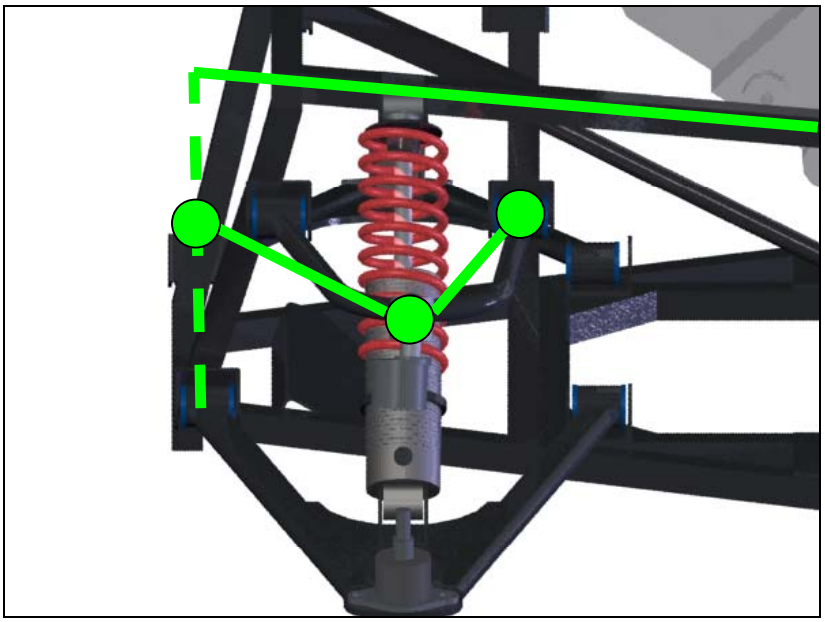

Figure 13: Modification to the front wishbone

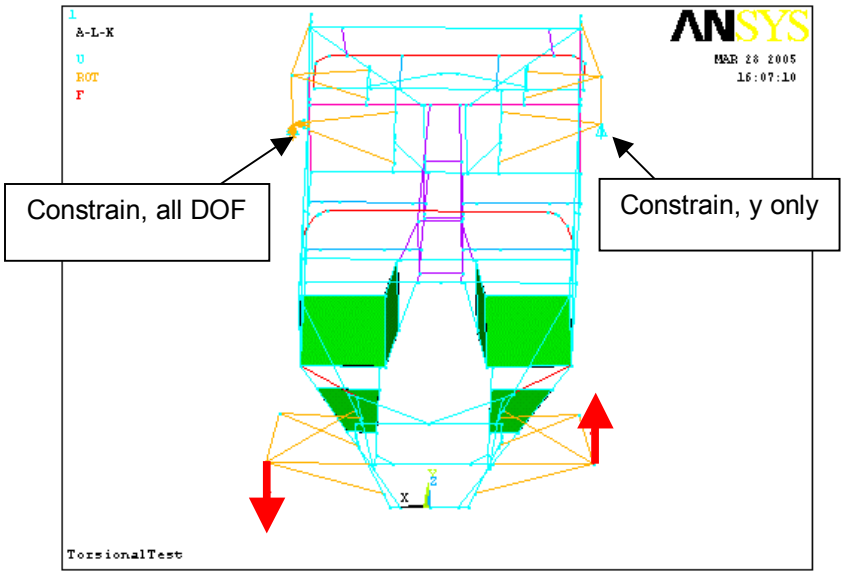

Figure 14: The pure torsion load case

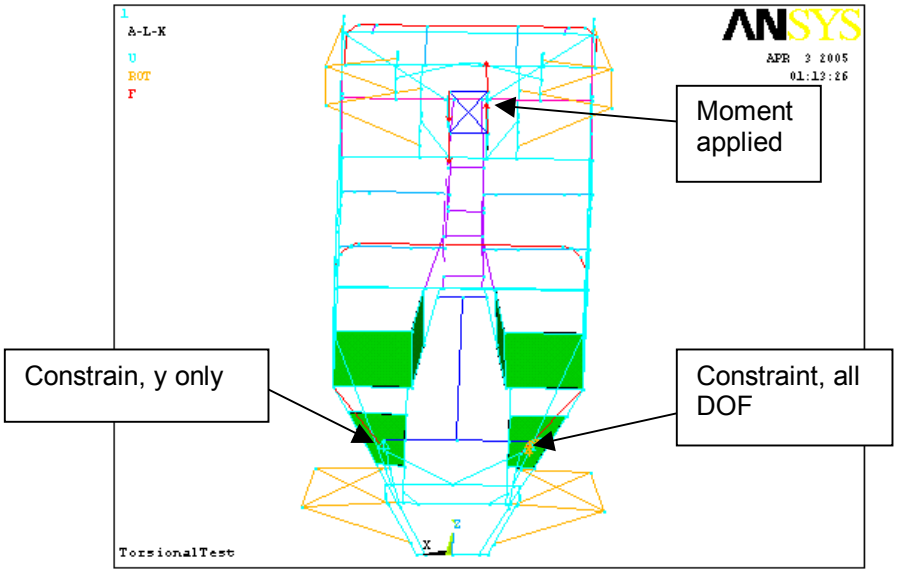

Figure 15: The engine torque load case

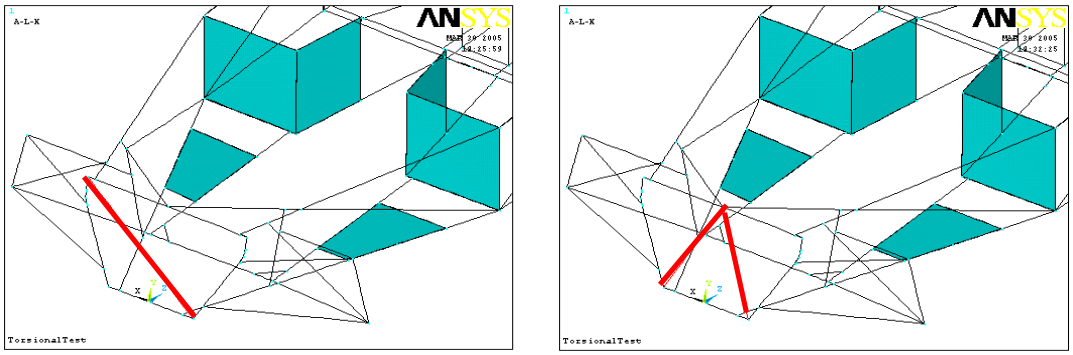

Figure 16: Front bulkhead triangulation 1 (left) and 2 (right)

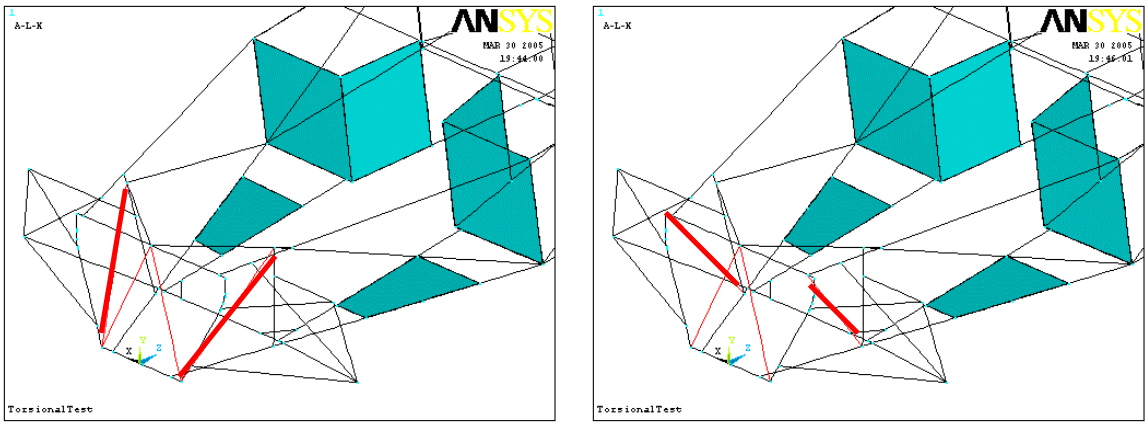

Figure 17: Wishbone mount triangulation 1 (left) and 2 (right)

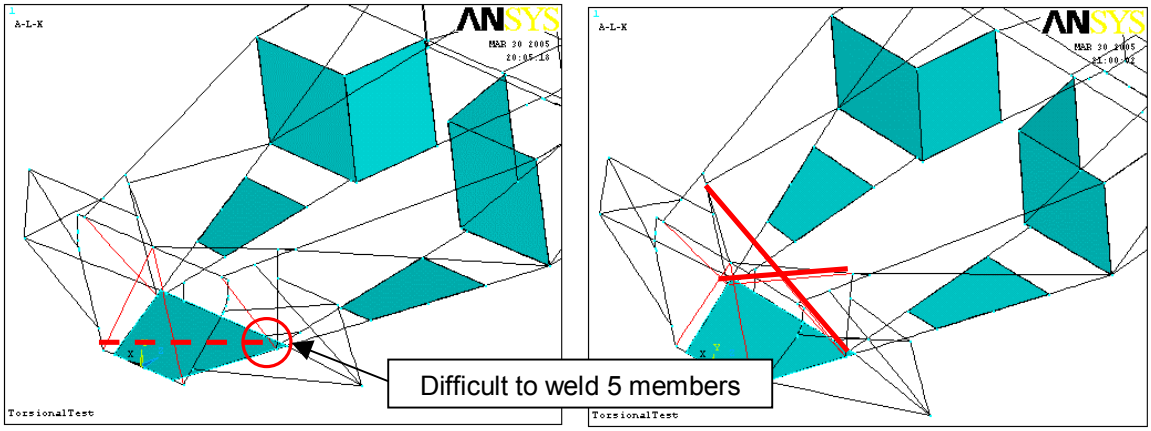

Figure 18: Plating the suspension box (left) and optional cross-brace (right)

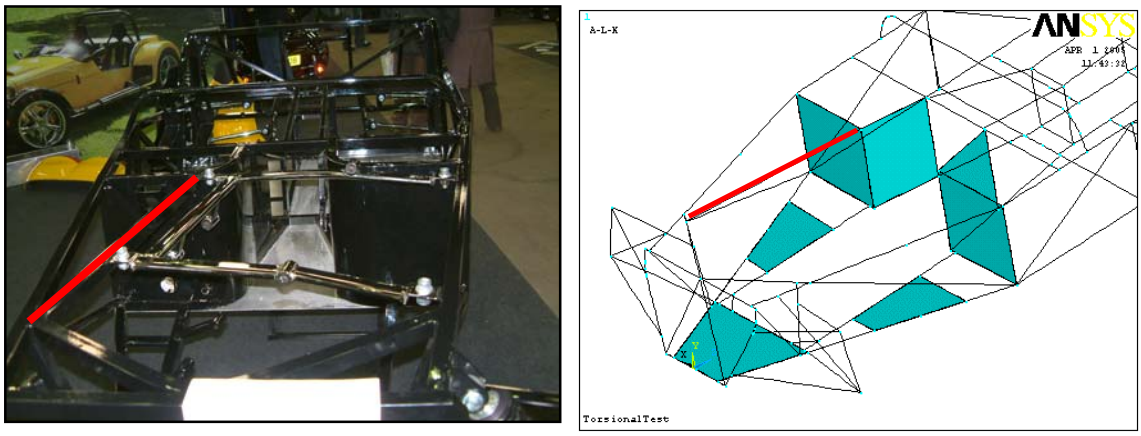

Figure 19: Single member R added

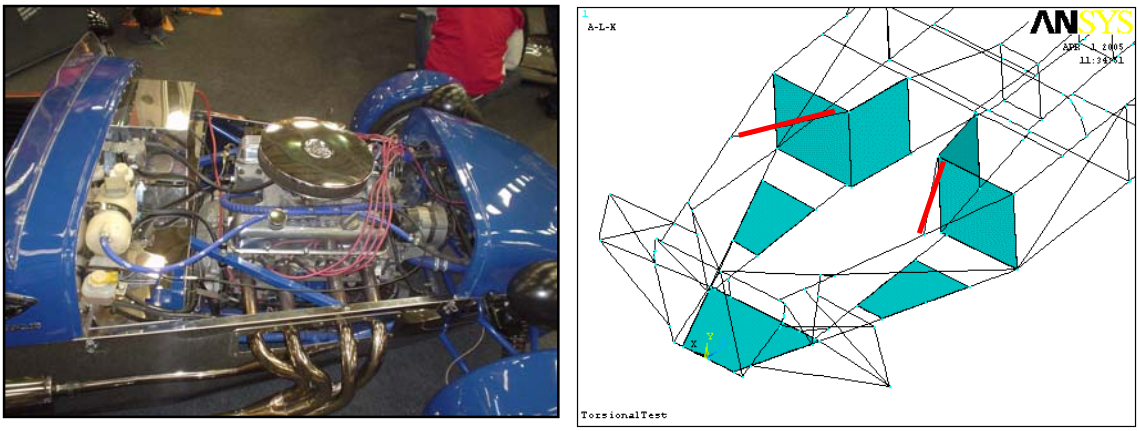

Figure 20: Two shorter member R's added to allow for V8 engine

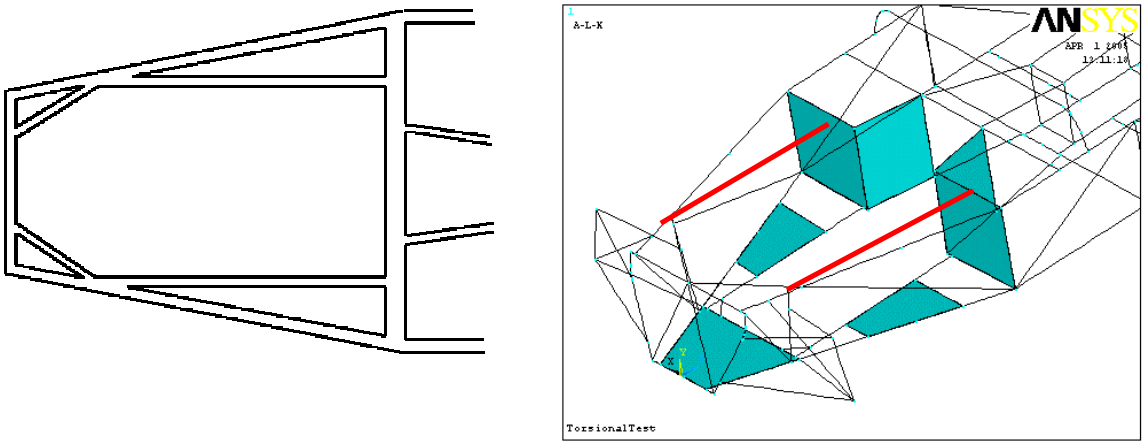

Figure 21: Longitudinal members added from the mid-span of the foot-wells

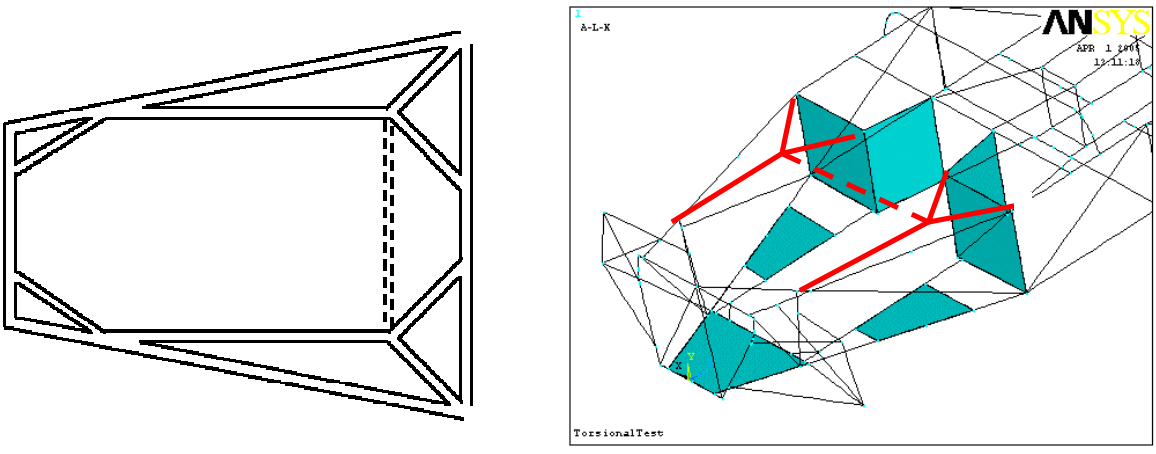

Figure 22: Y-braces

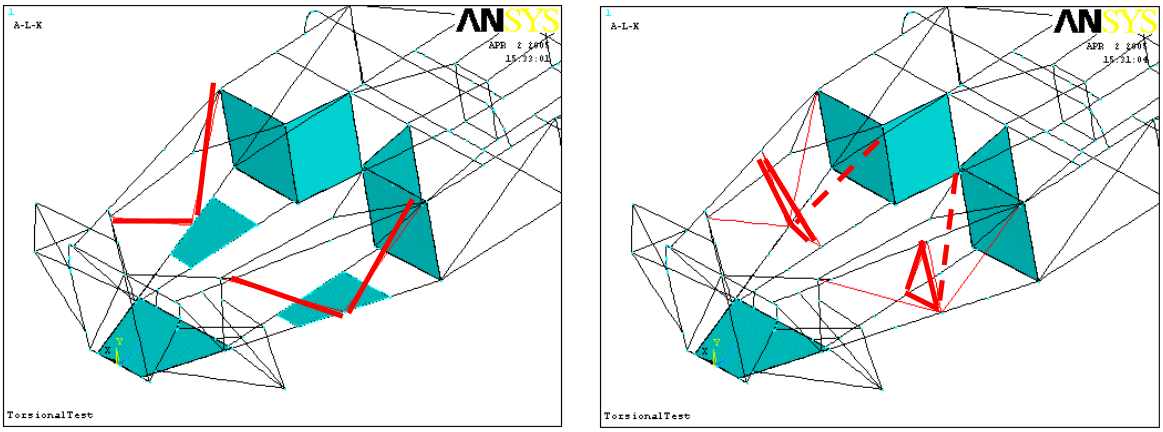

Figure 23: Engine bay side triangulation (left) and engine mount triangulation (right)

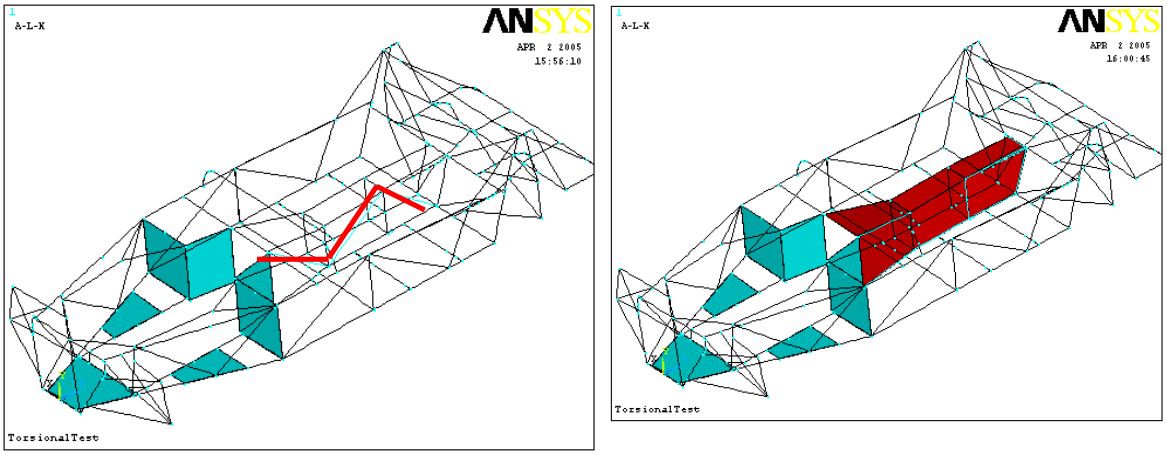

Figure 24: Triangulating the transmission tunnel (left) and plating the transmission tunnel (right)

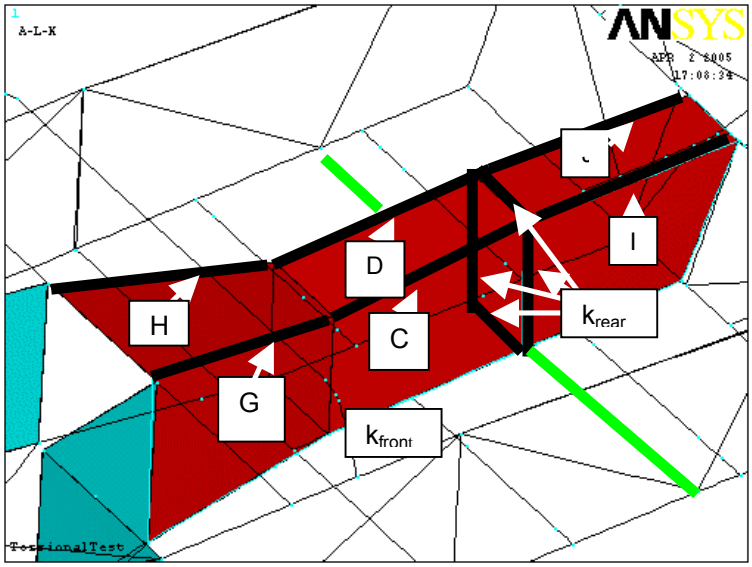

Figure 25: Plating the transmission tunnel creates 10 redundant members

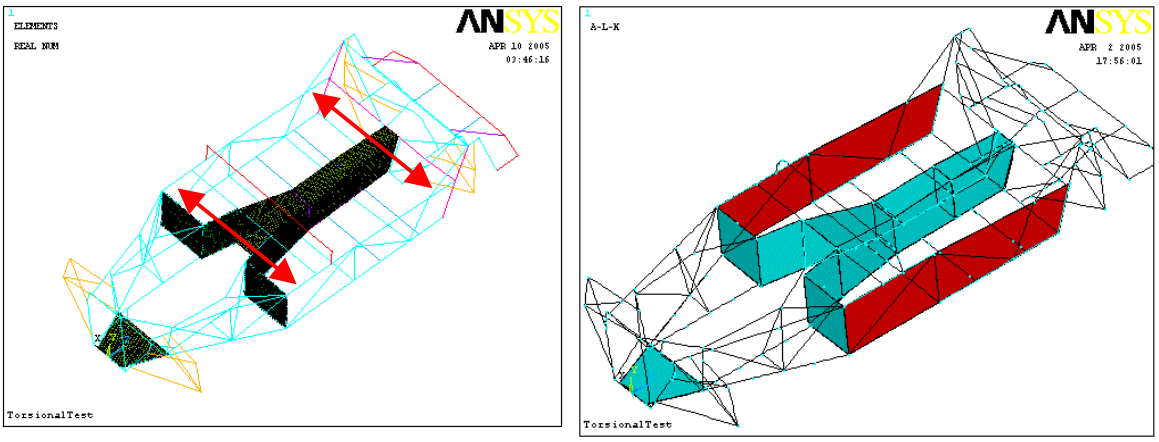

Figure 26: Widening the chassis 50mm either side (left) and side cladding (right)

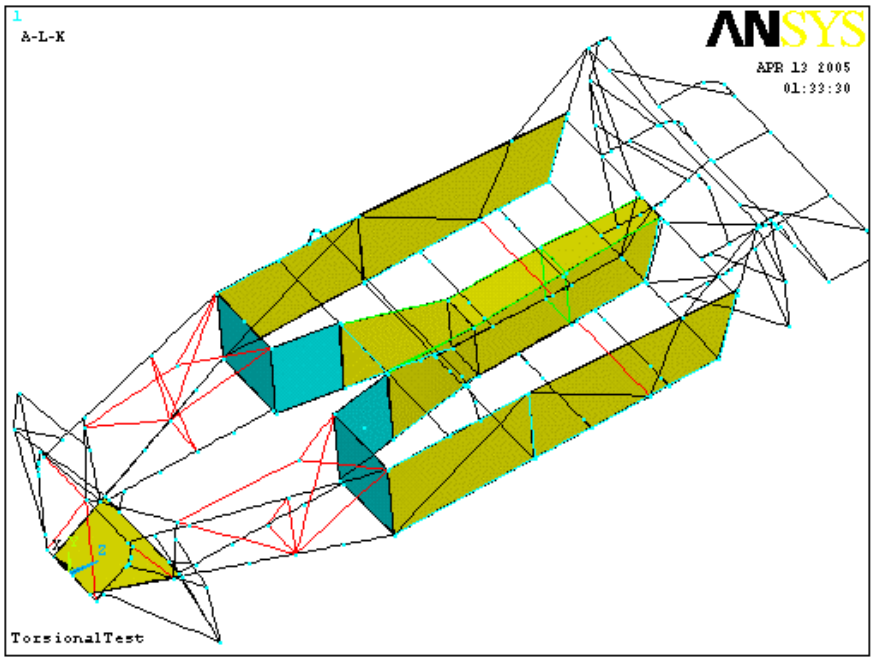

Figure 27: Modifications to the original chassis

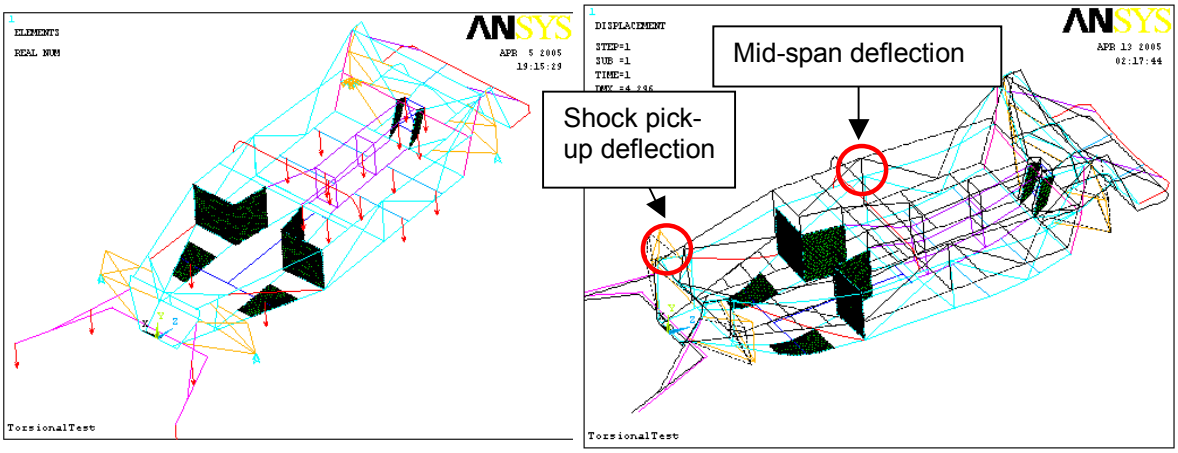

Figure 28: The vertical bending boundary conditions and loads (left) and the points of measurement (right)

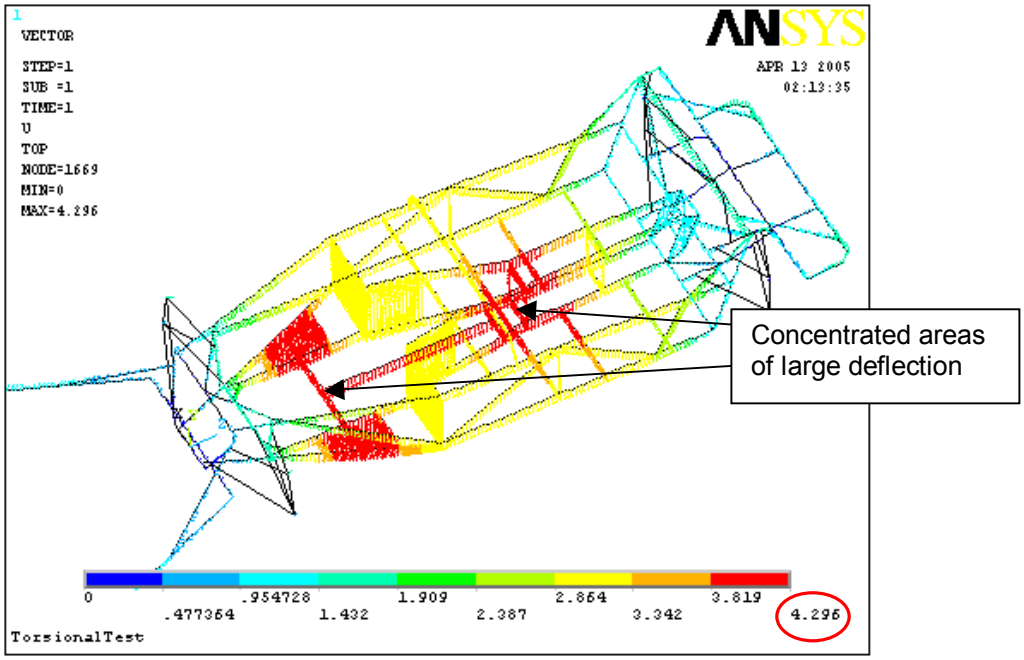

Figure 29: Deflection plot for original chassis subjected to vertical bending

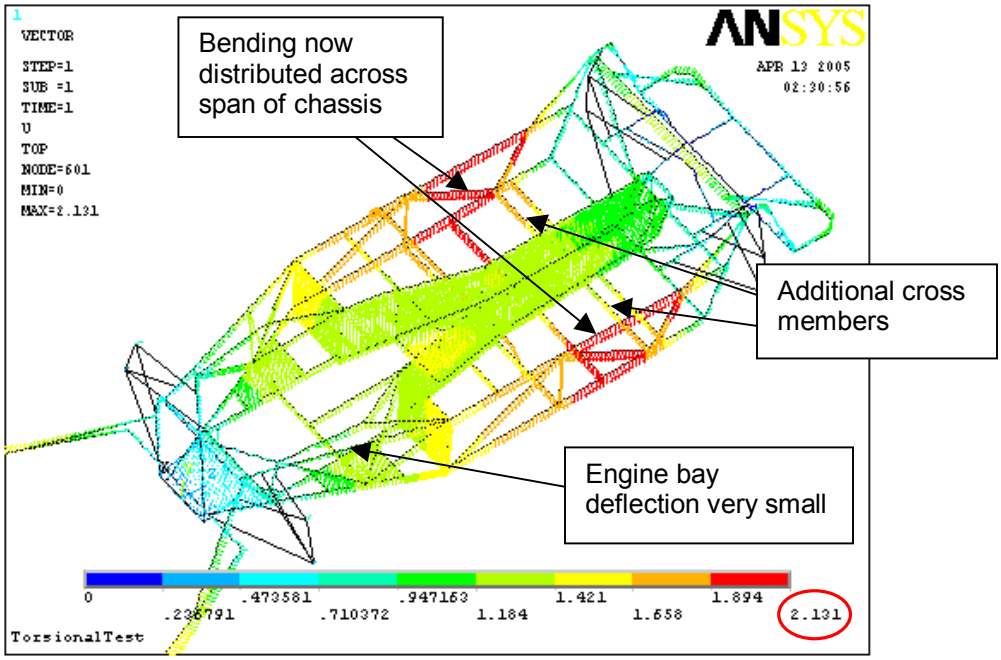

Figure 30: Deflection plot for modified chassis subjected to vertical bending